eNeuro

Research Article: New Research | Disorders of the Nervous System

Collapsin response mediator protein 4 (CRMP4) facilitates Wallerian degeneration and axon regeneration following sciatic nerve injury

https://doi.org/10.1523/ENEURO.0479-19.2020

Cite as: eNeuro 2020; 10.1523/ENEURO.0479-19.2020

Received: 18 November 2019
Revised: 14 January 2020
Accepted: 15 January 2020

Title: Collapsin response mediator protein 4 (CRMP4) facilitates Wallerian degeneration and axon regeneration following sciatic nerve injury

Marie-Pier Girouard[1], Tristan Simas[1], Luyang Hua[1], Barbara Morquette[1], Mohamad R. Khazaei[1], Nicolas Unsain[2], Aaron D. Johnstone[1], Isabel Rambaldi[1], Ricardo L. Sanz[1], Marie-Eve Di Raddo[3], Kanchana K. Gamage[4], Yu Yong[4], Dianna E. Willis[5], Valerie M.K. Verge[6], Philip A. Barker[1,7], Christopher Deppmann[4], Alyson E. Fournier[1]

[1]Department of Neurology & Neurosurgery, Montréal Neurological Institute, Montréal, QC, Canada, H3A 2B4

[2]Instituto de Investigación Médica Mercedes y Martín Ferreyra (INIMEC), Consejo Nacional de Investigaciones Científicas y Técnicas (CONICET), Córdoba, Argentina

[3]McGill University, Montréal, QC, Canada, H3A 0G4

[4]Department of Biology, University of Virginia, Charlottesville, VA, USA, 22903

[5]Brain and Mind Research Institute, Weill Cornell Medicine, Burke Institute, White Plains, NY, USA, 10605

[6]Department of Anatomy, Physiology and Pharmacology, University of Saskatchewan-CMSNRC, Saskatoon, SK, Canada, S7N 5E5

[7]Department of Biology, University of British Columbia, Kelowna, BC, Canada, V1V 1V7

Abbreviated title: CRMP4 facilitates degeneration and regeneration

Corresponding author:
Alyson E. Fournier, Ph.D.
Montréal Neurological Institute
3801 University Street, BT-109, Montréal, QC, Canada, H3A 2B4
Telephone: (514) 398-3154
FAX: (514) 398-6547
E-mail: alyson.fournier@mcgill.ca

Conflict of interest: The authors declare no competing financial interests.

Acknowledgements: We thank Jeannie Mui and Lee Ann Monaghan from the Facility for Electron Microscopy Research (FEMR) of McGill University for their help with the preparation of semi-thin sciatic nerve sections. We also thank Andrés de Léon, Ricardo Alchini, and Camille Juzwik for technical advice throughout this research project. This work was supported by grants from the Canadian Institutes of Health Research (CIHR) and the McGill Training Program in Neuroengineering.

Abstract

In contrast to neurons in the central nervous system (CNS), damaged neurons from the peripheral nervous system (PNS) regenerate, but this process can be slow and imperfect. Successful regeneration is orchestrated by cytoskeletal reorganization at the tip of the proximal axon segment and cytoskeletal disassembly of the distal segment. Collapsin response mediator protein 4 (CRMP4) is a cytosolic phospho-protein that regulates the actin and microtubule cytoskeleton. During development, CRMP4 promotes growth cone formation and dendrite development. Paradoxically, in the adult CNS, CRMP4 impedes axon regeneration. Here, we investigated the involvement of CRMP4 in peripheral nerve injury in male and female *Crmp4*$^{-/-}$ mice following sciatic nerve injury. We find that sensory axon regeneration and Wallerian degeneration are impaired in *Crmp4*$^{-/-}$ mice following sciatic nerve injury. *In vitro* analysis of dissociated dorsal root ganglion (DRG) neurons from *Crmp4*$^{-/-}$ mice revealed that CRMP4 functions in the proximal axon segment to promote the regrowth of severed DRG neurons and in the distal axon segment where it facilitates Wallerian degeneration through calpain-dependent formation of harmful CRMP4 fragments. These findings reveal an interesting dual role for CRMP4 in proximal and distal axon segments of injured sensory neurons that coordinately facilitate PNS axon regeneration.

Significance statement

PNS neurons spontaneously regenerate after injury; however, functional deficits often arise as a result of slow or misguided repair. Regrowth of the proximal axon segment coordinated with efficient Wallerian degeneration is important for optimal recovery. CRMP4 is a cytoskeletal regulatory protein with growth-promoting functions in the developing nervous system and growth-inhibitory roles in damaged adult CNS neurons. Here, we identify a pro-regenerative role for CRMP4 in peripheral nerve regeneration through the coordinated regulation of both axon regrowth and Wallerian degeneration.

Keywords: Collapsin response mediator protein (CRMP), Wallerian degeneration, Neuronal regeneration, Calpain, Sciatic nerve injury, Sensory neurons

Introduction

PNS and CNS neurons respond differently to injury because of distinct extracellular environments at the lesion site and differences in intrinsic signalling. Regeneration of axotomized peripheral nervous system (PNS) neurons is supported by the expression of regeneration-associated genes (RAGs) and a growth-permissive environment, whereas injured central nervous system (CNS) neurons fail to re-express RAGs and encounter glial-derived inhibitors that impede regeneration (Huebner and Strittmatter, 2009; Mokarram and Bellamkonda, 2011; Mietto et al., 2015). Even in the PNS, long-distance regeneration is slow and recovery is often incomplete, resulting in the partial or complete loss of sensory and/or motor functions (Mokarram and Bellamkonda, 2011). A stereotypical sequence of events is initiated upon PNS injury. The proximal axon segment reforms a growth cone that drives axon extension and regeneration while the detached distal axon segment undergoes Wallerian degeneration and subsequent fragmentation (Waller, 1850; Erez and Spira, 2008; Kamber et al., 2009; Ghosh-Roy et al., 2010; Bradke et al., 2012). Phagocytosis of cellular debris further contributes to a growth-permissive environment (Bruck, 1997; Lewis and Kucenas, 2014; Brosius Lutz et al., 2017). Impaired regeneration of injured sensory and motor neurons in slow degenerating *Wld*^{s} mice suggests that optimal regeneration requires proper coordination of proximal axon repair and distal axon degeneration (Bisby and Chen, 1990; Brown et al., 1992; Brown et al., 1994). Thus, proteins regulating both processes could represent therapeutic targets for promoting recovery following PNS injury.

Collapsin response mediator proteins (CRMPs) are a family of cytosolic phospho-proteins that regulate cytoskeletal dynamics during development and after injury (Alabed et al., 2007; Khazaei et al., 2014; Nagai et al., 2015; Tan et al., 2015; Nagai et al., 2016). The CRMP4 family member has two splice isoforms referred to as CRMP4L (Long) and CRMP4S (Short) and is an important neuro-developmental molecule promoting axonal extension and dendrite branching (Quinn et al., 2003; Niisato et al., 2012; Khazaei et al., 2014; Tan et al., 2015; Cha et al., 2016). However, in the adult CNS, CRMP4 null mice exhibit enhanced neuronal regeneration and reduced inflammation following spinal cord injury suggesting that CRMP4 impedes regeneration in this context (Nagai et al., 2015; Nagai et al., 2016). The inhibitory role of CRMP4 is partly due to its function in transducing signals from myelin-associated inhibitors (MAIs) and chondroitin sulfate

proteoglycans (CSPGs) (Alabed et al., 2007). In the adult mammalian PNS, CRMP4 is upregulated following sciatic nerve injury, but its function has not been investigated (Jang et al., 2010).

Here, we investigated the function of CRMP4 in response to PNS injury. We found that *Crmp4* deletion impaired the regeneration of sensory PNS neurons and delayed Wallerian degeneration of the distal processes *in vitro* and *in vivo*. Degeneration of the distal processes was facilitated by the calpain-mediated generation of toxic CRMP4 fragments. We conclude that in contrast to its affect in CNS neurons, CRMP4 facilitates PNS axon regeneration by coordinately regulating the regrowth of injured axons and Wallerian degeneration of the disconnected distal process.

Material & Methods

Animals

Animal procedures were performed in accordance with the Canadian Council on Animal Care Guidelines, and approved by the McGill University Animal Care and Use Committee. *Crmp4*$^{+/-}$ mice were generated and maintained in a C57BL/6J background as described previously (Khazaei et al., 2014). *Crmp4*$^{-/-}$ mice and *Crmp4*$^{+/+}$ littermate controls were generated by inter-crossing *Crmp4*$^{+/-}$ mice. *Caspase-3*$^{-/-}$ were obtained from Jackson Laboratory (strain B6.129S1-Casp3tm1Flv/J). Embryonic day 15-16 (E15-16) and postnatal day 4-7 (P4-7) C57BL/6 wild-type mice and Sprague-Dawley rats were provided by Charles River Laboratories.

Antibodies

The following antibodies were used for immunostaining and Western immunoblots: rabbit anti-stathmin-2/STMN2 (Novus Biologicals; catalog #NBP1-49461; RRID: AB_10011569), mouse anti-tubulin β3 (TUBB3) (clone TUJ1; Biolegend; catalog #801202; RRID: AB_10063408), mouse anti-tubulin β3 (TUBB3) (clone TUJ1; Millipore; catalog #AB9354; RRID: AB_570918), purified rabbit anti-tubulin β3 (clone Poly18020; Biolegend; catalog #802001; RRID: AB_2564645), mouse alpha-tubulin (Sigma-Aldrich; catalog #T9026; RRID: AB_477593), rabbit CRMP4 a/b (prepared in-house; (Alabed et al., 2007)), mouse α-fodrin (clone AA6; Enzo Life Sciences; catalog #BML-FG6090; RRID: AB_10554860), mouse anti-His antibody (QIAGEN; catalog #34670; RRID: AB_2571551), anti-GST rabbit antibody (generously

provided by the laboratory of Peter McPherson, Montreal Neurological Institute), mouse anti-rat CD68 conjugated to Alexa-Fluor 647 (Bio-Rad; catalog #MCA341A647; RRID: AB_566874), anti-neurofilament 200kDa conjugated to Alexa-Fluor 555 (clone NE14; Millipore; catalog #MAB5256A5; RRID: AB_2631099), anti-S-100 protein (clone 15E2E2; Millipore; catalog #MAB079-1; RRID: AB_571112), Alexa-Fluor 488-conjugated goat anti-mouse antibody (Thermo Fisher Scientific; catalog #A11001; RRID: AB_2534069), Fluorescein-conjugated goat anti-rabbit antibody (Thermo Fisher Scientific; catalog #F2765; RRID: AB_2536525), Alexa-Fluor 568-conjugated goat anti-rabbit antibody (Thermo Fisher Scientific; catalog #A11011; RRID: AB_143157), Alexa-Fluor 568-conjugated goat anti-mouse antibody (Thermo Fisher Scientific; catalog #A11031; RRID: AB_144696), horse-radish peroxidase (HRP)-conjugated anti-mouse IgG antibody (Jackson ImmunoResearch Labs; catalog #115-035-003; RRID: AB_10015289), and HRP-conjugated anti-rabbit IgG antibody (Jackson ImmunoResearch Labs; catalog #111-035-003; RRID: AB_2313567).

Plasmids and mutagenesis

Cloning of pcDNA3 CRMP4S-WT, and pET TAT v1 TAT-RFP were previously described (Alabed et al., 2007; Khazaei et al., 2015). To generate a pcDNA3 CRMP4S-T524A construct, the T524A mutation was introduced in pcDNA3 CRMP4S-WT using the Quik Change II XL site-directed mutagenesis kit (Agilent Technologies). To create a DNA construct encoding CRMP4 NTF and CTF, the nucleotide sequence corresponding to amino acids 1-520 or 521-570 of pcDNA3 CRMP4S-WT respectively was amplified by polymerase chain reaction (PCR). The resulting sequences were introduced in a pET TAT v1 vector or in a pGEX-4T-1 vector using restriction enzymes.

Purification of TAT peptides

TAT-RFP peptides were produced from Chinese hamster ovary (CHO) cells as described previously (Khazaei et al., 2015). To generate TAT-CRMP4 NTF and CTF peptides, BL21 bacterial cultures expressing pET Tat v1 CRMP4-NTF or -CTF were induced overnight with 1mM IPTG. The induced cultures were centrifuged and the pellet was resuspended in ice-cold buffer A (10 mM Tris-HCl pH 7.5, 600 mM NaCl, 20 mM imidazole, 1X complete protease inhibitors). The cell lysate was sonicated and cleared by ultracentrifugation. The cleared

supernatant was applied to a Ni-NTA column equilibrated with buffer A. The column was washed with buffer A and the proteins were eluted with buffer B (20 mM Tris-HCl pH 7.5, 1 M NaCl, 250 mM imidazole). The buffer in the eluate was exchanged to buffer C (20 mM $NaKPO_4$ pH 6.8, 600 mM NaCl, 5% glycerol) using a PD-10 column (GE Healthcare). The eluate was then applied to a 30S IEX column equilibrated with buffer D (10 mM $NaKPO_4$ pH 6.8, 300 mM NaCl, 2.5% glycerol). Finally, the column was washed with buffer D and eluted with buffer E (10 mM $NaKPO_4$ pH 6.8, 1.5 M NaCl, 2.5% glycerol). The eluate was concentrated on Amicon Ultra-4 3K or 10K Centricon column (EMD Millipore), aliquoted and stored at -80°C.

Purification of GST-CRMP4 NTF proteins

The purification of GST-CRMP4 protein was performed as described previously (Khazaei et al., 2014). Briefly, GST-CRMP4 NTF and GST as a control were expressed in *Escherichia coli* BL21 strain by induction with 0.5 mM IPTG. Bacterial pellets were then resuspended in lysis buffer (50 mM Tris-HCl pH 7.5, 50 mM NaCl, 5 mM $MgCl_2$, 1 mM DTT, protease inhibitors) and lysed by sonication (3 times at 50% amplitude for 30 sec). The clarified lysate was incubated with Glutathione-agarose beads (GE Healthcare Bio-Sciences) for 2 h at 4°C. Beads were then washed in washing buffer (50 mM Tris-HCl pH 7.5, 150 mM NaCl, 5 mM $MgCl_2$, 1 mM DTT) and were eluted with 20mM glutathione in elution buffer (50 mM Tris-HCl pH 8.0, 150 mM NaCl, 5 mM $MgCl_2$, 1 mM DTT). The eluate was concentrated on a Amicon Ultra-4 30K Centricon column concentrator (Millipore). Samples were aliquoted and stored at -80°C.

Culture of dissociated dorsal root ganglion (DRG) neurons

E15-16 and P4-7 rodent DRGs were dissected in ice-cold Leibovitz (L-15) medium (Thermo Fisher Scientific). The DRGs were dissociated in 0.25% Trypsin-EDTA (Thermo Fisher Scientific) at 37°C, gently triturated with a P1000 pipette tip, and resuspended in DRG media (Neurobasal (Thermo Fisher Scientific), 1% B27 (Thermo Fisher Scientific; catalog #17504-044), 1% N2 (Thermo Fisher Scientific; catalog #17502-048), 1% penicillin-streptomycin (Life Technologies; catalog #15140-122), 2 mM L-glutamine (Life Technologies; catalog #25030-081), 10 µM 5-fluoro-2'-deoxyuridine (FDU; Sigma-Aldrich; catalog #F0503)) supplemented with 50 $ng.ml^{-1}$ nerve growth factor (NGF; Cedarlane; catalog #CLMCNET-001). The dissociated DRG neurons were seeded onto culture plates or in microfluidic devices pre-coated with 100 $\mu g.ml^{-1}$

poly-L-lysine (PLL; Sigma-Aldrich; catalog #P1399) and 5-10 µg.ml^{-1} laminin (Corning; catalog #354232).

Preparation of Nogo-22 and treatment of DRG cultures

Production of Nogo-22 kDa protein was done as described previously (Huebner et al., 2011). Dissociated P4-7 rat DRG neurons were treated for 5 h with 600 ng GST-Nogo-22 or GST as a control. Lysates were prepared by collecting the treated DRGs in RIPA lysis buffer (50 mM Tris-HCl pH 7.4, 150 mM NaCl, 5 mM EDTA, 1% Triton X-100, 0.1% sodium deoxycholate, 0.1% SDS, 1 mM Na_3VO_4, 5 mM NaF, 1X complete protease inhibitors). The protein concentration in the lysates was normalized prior to analysis by Western blot.

In vitro ***regeneration of DRG axons in microfluidic devices***

Dissociated E15-16 mouse DRG neurons were seeded at a density of 10000-15000 neurons in microfluidic neuro devices (ANANDA devices) adhered to 3.5 cm imaging dishes (MatTek) pre-coated with 100 µg.ml^{-1} PLL and 5 µg.ml^{-1} laminin. At 4 days *in vitro* (DIV), the axons projecting to the bottom compartment were stained with 4 µl of 10 µM Mitotracker Green FM (Invitrogen; catalog #M7514) for 30 min. They were then axotomized by increasing the flow of medium in the bottom compartment of the microfluidic device using simultaneous vacuum aspiration and medium replacement to shear the axons. At 24 h following the axotomy, the neurons were fixed and stained with anti-tubulin β3 (TUBB3) antibody (1:1000) and Alexa-Fluor 568-conjugated secondary antibody (1:1000). Fluorescent images of the samples were acquired using an Axiovert1 microscope (Zeiss) with a 20X objective (Plan-APOCHROMAT Pln Apo 20X/0.8; Zeiss). Regrowth of the axons after axotomy was measured by manually tracing the axons with the NeuronJ plugin for ImageJ (Meijering et al., 2004). The extent of regeneration was measured by dividing the total neuronal regrowth in the bottom compartment of the microfluidic device by the number of channels with growing axons.

Treatment of DRG neurons grown in microfluidic devices with TAT- or GST-CRMP4 peptides

Dissociated E15-16 mouse DRG neurons were seeded at a density of 17000-25000 neurons in microfluidic neuro devices (ANANDA devices) adhered to a 3.5 cm imaging dish (MatTek) pre-coated with 100 µg.ml^{-1} PLL and 5 µg.ml^{-1} laminin. At 3 DIV, the axons projecting to the bottom

compartment of the microfluidic devices were treated for 8 h with 2.5 µM TAT-CRMP4-His-V5 peptides, GST-CRMP4 NTF peptides, or with TAT-RFP or GST as controls. The neurons were then fixed, and stained with anti-tubulin β3 (TUBB3) rabbit antibody (1:1000), anti-His mouse antibody (1:500), anti-GST rabbit antibody (1:500), and Alexa-Fluor conjugated secondary antibodies (1:1000). Fluorescent images of the samples were acquired using an Axiovert1 microscope (Zeiss) with a 20X objective (Plan-Apochromat Pln Apo 20X/0.8; Zeiss). The extent of degeneration was measured in at least 3 representative regions of interest (400 µm X 400 µm) per explant by calculating the index of degeneration, which corresponds to the area covered by the axonal fragments with a circularity above 0.9 divided by the total area covered by the axons (Kilinc et al., 2011).

Axotomy-induced degeneration of E12.5 DRG explants

Axotomy-induced degeneration of E12.5 mouse DRG explants was performed as previously described (Unsain et al., 2014). Briefly, the DRG explants were seeded onto cell-filter inserts coated with 1 $mg.ml^{-1}$ PLL, 10 $ug.ml^{-1}$ laminin and 0.1 $mg.ml^{-1}$ collagen, filled with DRG media with the bottom compartment supplemented with 15 $ng.ml^{-1}$ NGF. After approximately 60 h of growth, the explants on the upper side of the cell-filter inserts were detached with a cell scraper, and the axotomized axons were left to degenerate for 3 h after which they were collected in Laemmli sample buffer for subsequent analysis by Western blot. In some experiments, the DRG explants were treated with 5-15 µM ALLN (EMD Millipore; catalog #208719) prior to the axotomy. Alternatively, the DRG explants were grown on coated cell culture plates containing DRG media supplemented with 10 $ng.ml^{-1}$ NGF for approximately 60 h. The axons of the DRG explants were sectioned with a scalpel blade, and the axotomized axons were allowed to degenerate for 5 h to 5.5 h. The DRG explants were then fixed and stained with anti-tubulin β3 (TUBB3) antibody (1:1000) and Alexa-Fluor 568-conjugated secondary antibody (1:1000). The axotomized DRG explants were imaged with an Axiovert 200M microscope (Zeiss) using a 10X objective (CP-ACHROMAT 10X/0.25 Ph1; Zeiss). The extent of degeneration was measured in at least 3 representative regions of interest per explant (400 µm X 400 µm) by calculating the index of degeneration, which corresponds to the area covered by the axonal fragments with a circularity above 0.9 divided by the total area covered by the axons (Kilinc et al., 2011).

NGF withdrawal from E12.5 DRG explants

This experiment was conducted as previously described using E12.5 mouse explants (Unsain et al., 2014). Briefly, the E12.5 DRG explants were seeded into 6-well plates pre-coated with 1 $mg.ml^{-1}$ PLL, 10 $ug.ml^{-1}$ laminin and 0.1 $mg.ml^{-1}$ collagen in DRG media supplemented with 10 $ng.ml^{-1}$ NGF. After approximately 2 days of growth, the media was exchanged to NGF-free DRG media supplemented with 1 $ug.ml^{-1}$ anti-NGF antibodies. NGF withdrawal-induced degeneration was allowed to proceed for 24 h, after which the NGF-deprived axons were fixed and stained with anti-tubulin β3 (TUBB3) antibody (1:10000) and Alexa-Fluor 568-conjugated antibody (1:5000). The axons were imaged at a 5X magnification using a Zeiss Axioscope 2 microscope. The quantification of the area covered by the axons was done with Axoquant 2.0 in R Studio as previously described (Johnstone et al., 2018).

Immunostaining of dissociated DRG neurons and DRG explants

The dissociated DRG neurons or DRG explants were fixed for 30 min with 4% paraformaldehyde (PFA) diluted in phosphate-buffered saline (PBS) then thoroughly washed with PBS. The neurons were then permeabilized for 5 min with 0.2% Triton X-100/PBS prior to blocking in 5% bovine serum albumin (BSA) diluted in PBS for 1 h at room temperature. The neurons were then stained with primary antibody diluted in 5% BSA/PBS overnight at 4°C. The next day, the samples were washed in PBS, incubated in secondary antibody diluted in 5% BSA/PBS for 2 h at room temperature, and washed again in PBS.

Sciatic nerve injury

Male and female mice aged 3-4 months old were used for the sciatic nerve injuries. Following anesthesia with isoflurane, the sciatic nerve was exposed with a mid-thigh incision and crushed with a smooth-jaw hemostat (0.6 mm tip; Fine Science Tools) fully closed for 30 s at approximately 1 cm distal to the sciatic notch. The injury site was labeled by attaching a 9-0 non-absorbable silk suture (Ethicon) to the epineurium. Alternatively, the sciatic nerve was transected with straight semi-fine scissor (Fine Science Tools) and the nerve ends were pulled apart to prevent regeneration. Analgesia was managed by injecting buprenorphine (0.10 $mg.kg^{-1}$) subcutaneously and providing carprofen-containing MediGel CPF (ClearH_2O) *ad libitum*.

289 Animals were also given enrofloxacin (5 mg.kg^{-1}) subcutaneously pre- and post-operatively to
290 prevent infection.
291
292 ***Optic nerve injury***
293 Male and female mice aged 2-3 months old were used for optic nerve transection. Following
294 anesthesia with isoflurane, the optic nerve was exposed with an incision above the ocular orbit
295 and the extra-ocular muscles were resected. The optic nerve was transected with semi-fine
296 scissors (Fine Science Tools) at 0.5-1.0 mm from the optic nerve head. Care was taken to avoid
297 damage to the ophthalmic artery and the vascular integrity of the retina was assessed by fundus
298 examination. Analgesia was provided by subcutaneous injections of buprenorphine (0.05 mg.kg^{-}
299 ^{1}).
300
301 **In vivo *analysis of neuronal regeneration in whole-mount stained sciatic nerves***
302 At 3 days post-injury (DPI), mice were euthanized with isoflurane and CO_2 inhalation followed
303 by cervical dislocation. The injured and contralateral intact sciatic nerves were harvested and
304 fixed in 4% PFA/PBS for 5 h at 4°C. Following fixation, the tissues were washed in PBS, then
305 dehydrated in sequential washes of 50%, 80%, and 100% methanol (Sigma-Aldrich) for 1 h each
306 at room temperature, before quenching the endogenous peroxidase activity overnight at 4°C with
307 ice-cold H_2O_2 diluted in 20% DMSO/methanol (1 vol 30% H_2O_2, 1 vol DMSO, 4 vol methanol).
308 The following day, the tissues were rehydrated in a reversed gradient of methanol followed by
309 two washes of 1 h in PBS. Blocking was done overnight at 4°C in blocking buffer (10% normal
310 goat serum (NGS), 10% DMSO (Sigma-Aldrich), 0.2% Triton X-100 (Sigma-Aldrich), PBS).
311 The sciatic nerves were then stained sequentially with anti-stathmin-2 (STMN2; also referred to
312 as superior cervical ganglion 10 (SCG10; 1:200)) primary antibody and Alexa-Fluor 568-
313 conjugated goat anti-rabbit secondary antibody (1:200) diluted in antibody dilution buffer (3%
314 NGS, 5% DMSO, 0.2% Triton X-100, 10 ug.ml^{-1} heparin, PBS) for 7 days at 37°C to label the
315 regenerating sensory axon front as the anti-STMN2/SCG10 antibody preferentially detects
316 regenerating sensory and not motor axons (Shin et al., 2014). Following each incubation, the
317 nerves were thoroughly washed in 0.2% Triton X-100/PBS for 7 h at room temperature, changing
318 the wash buffer every hour. A final overnight wash was done in PBS before tissue clarification.
319 Prior to imaging, the stained nerves were cleared following an adapted 3DISCO protocol (Erturk

et al., 2012). Briefly, the nerves were dehydrated in a stepwise gradient of 50%, 80% and 100% tetrahydrofuran (THF; Sigma-Aldrich) diluted in distilled water. The nerves were then cleared by immersion in dibenzyl ether (DBE; Sigma-Aldrich). The whole nerves were imaged with a SP8 confocal laser-scanning microscope (Leica) using a 10X objective (HC PL APO 1.x/0.40 CS). The distance of regeneration was measured as described previously (Leon et al., 2000). Briefly, the number of SCG10+ neurons located at 500 µm increments from the injury site were counted in alternating optical sections. The resulting number was divided by the diameter of the nerve (mm) to calculate the number of axons per mm for each section counted. The number of axons/mm was then averaged over all the sections. Finally, the total number of axons $\sum a_d$ extending to a distance d was estimated by summing all sections: $\sum a_d \approx \pi r^2 \cdot (average\ axons/mm)/t$, where r is the radius of the nerve and t is the optical thickness of the sections.

In vivo *analysis of axonal degeneration in sciatic nerves*

The mice were euthanized by intracardial perfusion with ice-cold 4% PFA. The nerve stump distal to the injury site and the corresponding contralateral nerve were harvested and post-fixed in 2.5% gluteraldehyde in 0.1 M PBS. Post-processing of the nerve samples was conducted by the Facility for Electron Microscopy Research (FEMR) of McGill University. Briefly, the fixed sciatic nerves were stained with 1% osmium tetroxide, dehydrated in sequential washes with a gradient of ethanol and embedded in epoxy embedding medium (Electron Microscopy Sciences). Semi-thin transverse nerve sections with a thickness of 0.5 µm were prepared using an ultramicrotome (Reichert) and mounted with a coverslip using Permount mounting medium (Fisher Scientific; catalog #SP15-100). Imaging was done with an Axiovert 200M epifluorescence microscope (Zeiss) using a 63X objective (Plan-Neofluar 1.25 Oil; Zeiss). To evaluate the extent of degeneration, the number of intact axons per μm^2 was counted.

Tissue homogenization

At selected time points following nerve transection, the mice were euthanized with isoflurane and CO_2 inhalation followed by cervical dislocation. Sciatic nerve, optic nerve, L4-6 DRGs and retina samples were collected, washed briefly in ice-cold PBS, and manually homogenized in RIPA lysis buffer (50 mM Tris-HCl pH 7.4, 150 mM NaCl, 5 mM EDTA, 1% Triton X-100, 0.1%

sodium deoxycholate, 0.1% SDS, 1 mM Na_3VO_4, 5 mM NaF, 1X complete protease inhibitors). The protein concentration in the resulting sonicated and cleared lysates was measured and normalized between samples prior to analysis by Western immunoblot.

Overexpression of CRMP4 in HEK 293T cells and in vitro digestion with recombinant calpain

HEK 293T cells maintained in DMEM medium supplemented with 10% fetal bovine serum (FBS) were transfected using Lipofectamine 2000 (Invitrogen) following manufacturer's instruction. The cells were washed briefly in ice-cold PBS and lysed with RIPA lysis buffer (50 mM Tris-HCl pH 7.4, 150 mM NaCl, 5 mM EDTA, 1% Triton X-100, 0.1% sodium deoxycholate, 0.1% SDS, 1 mM Na_3VO_4, 5 mM NaF, 1X complete protease inhibitors). The protein concentration in the sonicated and cleared lysates was normalized. The lysates were digested *in vitro* with 1 unit of recombinant calpain-1 (EMD Millipore; catalog #208713) and 2 mM $MgCl_2$ for 30 min at 37°C. The digested proteins were then analyzed by Western blot. In some experiments, the calpain inhibitor 5-15 μM ALLN (EMD Millipore; catalog #208719) was added to the reaction.

Western blots

The protein content of tissue and cell lysates was analyzed by SDS-Page gel separation followed by Western immunoblot. PVDF membranes were blocked with 5% milk diluted in Tris-buffered saline (TBS) supplemented with 0.05% Triton X-100 for 1 h at room temperature, probed with primary antibody overnight at 4ºC and with secondary antibodies for 1 h at room temperature. The antibodies used were: rabbit CRMP4 a/b (1:7500), mouse α-fodrin (1:500), mouse anti-tubulin beta3 (1:5000), mouse alpha-tubulin (1:5000), and horse-radish peroxidase (HRP)-conjugated anti-mouse and anti-rabbit IgG antibodies (1:10000). The signal was revealed with Western Lightning Plus ECL (PerkinElmer). Quantification of the intensity of the bands was performed in Photoshop. Changes in CRMP4 expression in the cell body compartment was normalized to a tubulin loading control.

Statistical analysis

Statistical analyses were performed with the GraphPad Prism 8 software. Two-tailed Student t-test were used when directly comparing 2 conditions, while one-way analysis of variance

(ANOVA) followed by Tukey's multiple comparison tests were used when more than 3 conditions were compared. For experiments with more than one variable parameters such as the *in vivo* regeneration and degeneration experiments, a two-way ANOVA followed by Bonferroni's multiple comparison tests were used. Statistical details, p values and experimental details are indicated in the corresponding figure legends.

Results

Crmp4 *deletion impairs regeneration of sensory neurons following sciatic nerve injury*

Paradoxically, CRMP4 facilitates growth during development, but impedes regeneration of injured CNS neurons (Quinn et al., 2003; Alabed et al., 2007; Nagai et al., 2012; Niisato et al., 2012; Khazaei et al., 2014; Nagai et al., 2015; Tan et al., 2015; Nagai et al., 2016). Thus, we sought to investigate the functions of CRMP4 in regeneration-competent PNS neurons. Sciatic nerve crush injuries were performed on adult *Crmp4*$^{-/-}$ mice and littermate *Crmp4*$^{+/+}$ controls. Regenerating fibres were stained for SCG10, a protein that is preferentially upregulated in regenerating sensory neurons and their growth was evaluated at 3 days post-injury (DPI) (Mason et al., 2002; Shin et al., 2014). In both *Crmp4*$^{+/+}$ and *Crmp4*$^{-/-}$ sciatic nerves, SCG10+ neurons grew spontaneously across the injury site following sciatic nerve crush injury (Fig. 1A) However, quantification of the number of regenerating fibres at progressive distances from the lesion site revealed that sensory neurons in *Crmp4*$^{+/+}$ mice extend further than those in *Crmp4*$^{-/-}$ mice (Fig. 1B) revealing a pro-regenerative function for CRMP4 in the PNS, which contrasts to its inhibitory role in the CNS (Alabed et al., 2007; Nagai et al., 2012; Nagai et al., 2015; Nagai et al., 2016).

CRMP4 expression is differentially regulated in the CNS and PNS following injury

Next, we sought to determine whether the distinct regenerative phenotypes observed in the PNS and CNS could stem from differences in the expression profile of CRMP4. CRMP4 expression was assessed by Western blot analysis of lysates prepared from PNS and CNS cell bodies and axons. For analysis of the PNS, lumbar dorsal root ganglions (DRGs) containing the cell bodies of sensory neurons and sciatic nerves containing their axons were collected at 3 days following sciatic nerve transection (Fig. 2A). CRMP4 was robustly expressed in intact and injured DRGs with little change in expression following injury (Fig. 2B; CRMP4S expression 88 ± 12%

control). In the sciatic nerve, expression of the short CRMP4 isoform (CRMP4S) was markedly reduced in the nerve distal to the lesion site where axons undergo Wallerian degeneration (56 ± 1% of control levels) mirroring the regulation of tubulin (33 ± 8% of control), and bands representing the long isoform of CRMP4 (CRMP4L) and a truncated 55 kDa CRMP4 cleavage fragment (tCRMP4) became apparent (Fig. 2C). In the proximal segment of sciatic nerve where the growth cones of regenerating neurons reform, CRMP4S expression remained constant (94 ± 5% and 99 ± 3% in proximal 1 and proximal 2 segments, respectively) and CRMP4L was modestly upregulated (Fig. 2C). To determine the cell types expressing CRMP4, crushed sciatic nerves were stained with a pan-CRMP4 antibody. CRMP4 co-localized with the neuronal marker Tuj1 (Fig. 2D), but not with the Schwann cell marker S100 (Fig. 2E), or the macrophage marker ED1 (Fig. 2F). This reveals that CRMP4 is preferentially expressed in neurons suggesting a neuron cell-autonomous role following PNS injury.

We then analyzed the expression of CRMP4 in the damaged CNS, focusing on the retinal ganglion cells (RGCs) and the retina at 3 days after optic nerve transection (Fig. 2G). In the CNS, CRMP4 expression was unaltered in the retina 3 days following optic nerve transection (Fig. 2H; CRMP4S expression 101 ± 6% of control levels), similar to the CRMP4 expression pattern observed in DRG cell bodies. In the optic nerve, CRMP4 regulation was notably different from the sciatic nerve (Fig. 2I). In the optic nerve segments, truncated CRMP4 was apparent in the distal segment following optic nerve injury, but CRMP4S and CRMP4L expression was largely retained (CRMP4S 100 ± 1% of control). In the proximal segment of the damaged optic nerve, CRMP4S was strongly downregulated (31± 9% of control levels) with the appearance of tCRMP4 (Fig. 2I). Intriguingly, this reveals a distinct regulation of CRMP4 following injury to PNS versus CNS neurons. In the regenerating PNS, CRMP4 expression is retained in the proximal segment of sciatic nerve correlating with the regeneration of severed axons, whereas CRMP4 is downregulated in the proximal segment of optic nerve where axons fail to regrow. Further, in the distal sciatic nerve, CRMP4 is cleaved and downregulated, coinciding with the onset of Wallerian degeneration, while CRMP4 expression is largely retained at the same time point in the distal optic nerve. CRMP4 is also expressed in different cell types in the crushed optic nerve at 8 DPI, as it is expressed in the scar forming non-neuronal cells surrounding the

injury site (Fig. 2J). The distinct regulation of CRMP4 in injured PNS and CNS neurons led us to speculate that full-length CRMP4 in the proximal segment of injured PNS neurons may support regrowth whereas CRMP4 cleavage may contribute to Wallerian degeneration in the distal segment of sciatic nerve.

***CRMP4 enhances regrowth of injured sensory neurons* in vitro**

To test whether CRMP4 expression in the proximal segment of injured sensory neurons promotes axon extension after injury, we conducted a more extensive time course analysis of CRMP4 expression following sciatic nerve injury. Following sciatic nerve transection, CRMP4 expression is retained in the proximal nerve segment for up to 14 DPI (Fig. 3A). To test the cell-autonomous contribution of CRMP4 to the regrowth of damaged axons, we measure the extent of regeneration of axotomized DRG neurons *in vitro*. DRGs were isolated from E15-16 wild-type or *Crmp4*$^{-/-}$ mouse embryos and the dissociated neurons were plated in microfluidic devices for 4 days until the axons projected into the axonal compartment (Jones et al., 2006; Frey et al., 2015; Dubovy et al., 2018). Axotomy was then performed by increasing the flow of medium in the axonal compartment to shear the axons, and the damaged neurons were left to regenerate for 24 h. Following axotomy, *Crmp4*$^{-/-}$ DRG neurons regrew significantly worse than their wild-type counterparts, exhibiting 43% less regrowth (Fig. 3B, C). The regenerating CRMP4$^{-/-}$ neurites also adopted a curled phenotype, often looping back towards the channels, which differs from the straight outgrowth profile of wild-type neurons (Fig. 3B). This finding demonstrates that CRMP4 enhances the regrowth of the proximal tip of axotomized sensory neurons in a neuron cell-autonomous manner.

Crmp4 *deletion delays Wallerian degeneration in the PNS*

We next investigated whether CRMP4 might be involved in the regulation of Wallerian degeneration in the sciatic nerve. Previous studies have demonstrated that axon regeneration is impaired in mice with delayed Wallerian degeneration, suggesting that clearance of axon distal segments facilitate axon regeneration (Bisby and Chen, 1990; Brown et al., 1992; Brown et al., 1994). We first assessed Wallerian degeneration in the transected sciatic nerve by quantifying the number of intact myelin sheaths in semi-thin cross-sections of the nerve segment located distal to the injury site, an indirect measure of axon degeneration as Wallerian degeneration is followed by

degradation of myelin sheaths. The data revealed a higher number of intact myelinated sheaths in the sciatic nerve collected from *Crmp4*$^{-/-}$ mice compared to the *Crmp4*$^{+/+}$ controls at 36HPI, which became statistically significant at 3 DPI (Fig. 4A, B). By 7 DPI, the degradation of myelin sheaths was extensive in both *Crmp4*$^{+/+}$ and *Crmp4*$^{-/-}$ sciatic nerves. These results indicate that *Crmp4* deletion delays Wallerian degeneration following sciatic nerve injury.

To better understand the function of CRMP4 in Wallerian degeneration, we examined axon degeneration in an *in vitro* axotomy model (Gerdts et al., 2013; Gamage et al., 2017). E12.5 *Crmp4*$^{+/+}$ and *Crmp4*$^{-/-}$ DRG explants were grown for 60 h, prior to the neurites being sectioned with a blade and allowed to degenerate for 5 h. The index of degeneration of these neurites was then calculated by dividing the area covered by particles with a circularity above 0.9, which corresponds to the axon fragments, by the total area covered by the neurites (Kilinc et al., 2011). The quantification revealed that *Crmp4*$^{-/-}$ neurons have a lower index of degeneration compared to the *Crmp4*$^{+/+}$ neurons, illustrating a cell-autonomous role for CRMP4 in Wallerian degeneration (Fig. 4C, D). Interestingly the pro-degenerative function of CRMP4 following axotomy is not conserved in another model of degeneration; trophic factor deprivation. When E12.5 *Crmp4*$^{-/-}$ and *Crmp4*$^{+/+}$ DRG explants were deprived of nerve growth factor (NGF) and treated with anti-NGF antibody, they exhibited typical signs of degeneration, such as the appearance of axon swellings and fragments (Fig. 4E). The area covered by the neurites following degeneration was not significantly different between the NGF-deprived *Crmp4*$^{-/-}$ and *Crmp4*$^{+/+}$ DRG explants (Fig. 4F, G), indicating that the effect of CRMP4 on Wallerian degeneration is somewhat selective.

CRMP4 is cleaved by calpain in axotomized sensory neurons

We found that the expression of CRMP4 was downregulated in degenerating axons located distal to a sciatic nerve injury, coincident with the appearance of a truncated CRMP4 species. We thus sought to investigate the mechanism underlying the cleavage of CRMP4 and its contribution to Wallerian degeneration. CRMP family members including CRMP4 have been described as calpain substrates in response to ischemic and excitotoxic stimuli (Kowara et al., 2005; Kowara et al., 2006; Jiang et al., 2007; Zhang et al., 2007; Liu et al., 2009). To determine if calpain is active in the injured sciatic nerve, we investigated the cleavage of fodrin, a calpain substrate that

505 is alternatively referred to as αII-spectrin and that is often used as a marker of calpain activity
506 (Wang, 2000). Following injury, 145 kDa and 150 kDa spectrin breakdown products
507 characteristic of calpain-mediated cleavage were elevated in the distal sciatic nerve segment, but
508 largely unregulated in the proximal segment (Fig. 5A; (Wang, 2000)). The fragments were
509 detected at 1, 3 and 5 DPI and resolved by 14 DPI consistent with the time course of CRMP4
510 cleavage *in vivo* (Fig. 3A). Analysis of proximal and distal segments of optic nerve following
511 transection revealed fodrin cleavage in both the proximal and distal nerve segments (Fig. 5B),
512 consistent with the appearance of a CRMP4 cleavage product in proximal and distal optic nerve
513 (Fig. 2E). This data suggests that calpain could potentially cleave CRMP4 to generate tCRMP4 in
514 response to axotomy. To directly test this, P4-7 DRG neurons were treated with recombinant
515 calpain, which did indeed lead to the generation of a 55 kDa tCRMP4 cleavage fragment (Fig.
516 5C), supporting the idea that CRMP4 cleavage is a calpain-dependent process. We also asked if
517 generation of the CRMP4 cleavage product could be efficiently blocked with a calpain inhibitor.
518 DRG explants were grown on cell-filter inserts and axotomized by removing the cell bodies with
519 a cell scraper. The axons on the underside of the filter were then collected and lysed for Western
520 immunoblot. Severed axons revealed the presence of tCRMP4 and generation of this fragment
521 was efficiently blocked with the calpain inhibitor ALLN (Fig. 5D). Because calpains can activate
522 other enzymes that also contribute to degeneration such as caspases, we repeated the experiment
523 in DRG explants isolated from *Caspase 3*$^{-/-}$ mice (Geden and Deshmukh, 2016). Similar to the
524 wild-type DRG explants, axotomy-dependent cleavage of CRMP4 occurred in the axotomized
525 *Caspase 3*$^{-/-}$ axons and this was prevented by treatment with ALLN (Fig. 5E). These findings
526 illustrate that axotomy is sufficient to drive the process of calpain-dependent CRMP4 cleavage.
527
528 Further, to address how CRMP4 may be cleaved proximal and distal to the lesion site in optic
529 nerve while being restricted to the distal portion of the sciatic nerve, we asked if CNS myelin-
530 associated proteins affect CRMP4 cleavage. We found that treatment of P4-P7 DRG neurons
531 with Nogo-22, an outgrowth inhibitory fragment of the CNS myelin-associated inhibitor Nogo-A,
532 was sufficient to induce CRMP4 cleavage (Fig. 5F) (Huebner et al., 2011), This finding is
533 consistent with the finding that Nogo promotes calcium influx in neurons leading to the
534 activation of calpain (Bandtlow and Loschinger, 1997). This raises the possibility that calpain

activation and CRMP4 cleavage may occur both proximally and distally following optic nerve injury in response to Nogo while it may be more spatially restricted in the PNS environment.

CRMP4 cleavage fragments promote axon degeneration

To study the effects of CRMP4 cleavage fragments on neurons, we mapped the calpain cleavage site. Through sequential alanine substitutions of candidate residues in the carboxy-terminal tail of CRMP4, we localized the specific cleavage site to residue T524 and demonstrated that a CRMP4 construct containing a T524A mutation was less sensitive to *in vitro* calpain digestion (Fig. 6A). We then generated amino- and carboxy-terminal fragments of CRMP4 (CRMP4 NTF and CRMP4 CTF, respectively) as TAT peptides to mediate peptide internalization across the cell membrane (Fig. 6B, C; (Torchilin, 2008; Khazaei et al., 2015)). Dissociated wild-type E15-16 DRG neurons were grown in microfluidic devices and the axons were treated for 8 h with TAT-CRMP4 peptides or with TAT-RFP as a control. Treatment with either TAT-CRMP4 NTF or CTF resulted in significant axonal degeneration as characterized by the appearance of axonal swellings (Fig. 6D). The extent of degeneration was assessed by calculating the index of degeneration (Kilinc et al., 2011). This quantification revealed a significant effect of both CRMP4 fragments on axon degeneration compared to TAT-RFP (Fig. E; fold change of 5.19 for TAT-CRMP4 NTF and of 4.50 for TAT-CRMP4 CTF), indicating that CRMP4 cleavage is sufficient to promote axonal degeneration. Combined treatment with TAT-CRMP4 NTF and CTF resulted in a similar significant effect on axon degeneration, indicating that the combination is not more potent *in vitro* (fold-change of 6.89; p=0.231). Addition of GST-CRMP4 NTF, which lacks the TAT membrane permeabilization sequence, failed to affect axon degeneration (Fig. 6F).

Discussion

Following injury, peripheral neurons mount a regenerative response whereby a newly-formed growth cone at the tip of the broken axon drives axon outgrowth, while the disconnected axon segments undergo Wallerian degeneration (Waller, 1850; Kamber et al., 2009; Ghosh-Roy et al., 2010; Bradke et al., 2012; Spira and Erez, 2013). Neuronal regeneration and degeneration are highly inter-dependent, and as such, they share several signalling pathways (Bisby and Chen, 1990; Brown et al., 1992; Brown et al., 1994; Girouard et al., 2018). This is advantageous as both processes can be simultaneously targeted to promote an optimal regenerative response. Here, we

characterized CRMP4 as a protein that contributes to both regeneration and degeneration following axotomy. CRMP4 plays a dual role in the neuronal response to PNS injury, as loss of CRMP4 impairs sensory axon regeneration by limiting axon regrowth and delaying Wallerian degeneration. These findings ascribe to a novel pro-regenerative role to CRMP4 in the PNS, contrasting to its role in the CNS, where it contributes to failed regeneration. Interestingly, these functions are very reminiscent of other proteins that regulate cytoskeletal dynamics and energy supply (Girouard et al., 2018). For example, SCG10/STMN2 accumulates in the regenerating axon segment of sensory neurons following peripheral axotomy to promote microtubule dynamics and axon regrowth (Shin et al., 2014). Conversely, it is degraded in the degenerating axon segment to accelerate axon fragmentation (Shin et al., 2012).

Here, we find that, in the regenerating neurons, CRMP4 supports axon regrowth, while its calpain-mediated cleavage in the distal degenerating fibres facilitates Wallerian degeneration (Fig. 7B). It is notable that the relative ratio between full-length and truncated CRMP4 seems to be critical to its function (Fig. 7). In the injured PNS, full-length CRMP4 is exclusively expressed in the proximal segment correlating with axon regeneration. In the distal sciatic nerve, massive downregulation of full-length CRMP4 coinciding with the appearance of cleavage fragments correlates with Wallerian degeneration. In the optic nerve, CRMP4 expression in the proximal nerve segment mirrors the profile of the distal sciatic nerve and this correlates with the formation of retraction bulbs and failed regenerative growth. While CRMP4 cleavage also occurs in the distal optic nerve, full-length CRMP4 is retained and may dimerize with truncated CRMP4 to buffer its neurotoxic activity. This is consistent with the idea that overexpression of non-phosphorylated CRMP2 can protect axons from Wallerian degeneration (Wakatsuki et al., 2011).

Efficient neuronal regeneration requires the assembly of a functional growth cone that will drive axon extension (Bradke et al., 2012). This process is highly dependent on cytoskeletal remodeling and consequently, several cytoskeletal regulators are implicated in this process. Here, we find that CRMP4 contributes favorably to PNS regeneration and this effect potentially stems from its regulatory functions towards the cytoskeleton. To support this hypothesis, hippocampal neurons lacking CRMP4 exhibit poorly elaborated growth cones with defects in their cytoskeletal organization (Khazaei et al., 2014; Tan et al., 2015). Thus, CRMP4 could potentially facilitate the

cytoskeletal rearrangements required for the reformation of the growth cone, either via its direct interaction with actin and tubulin to promote their assembly into filaments or microtubules respectively, or via its interaction with CRMP2 (Rosslenbroich et al., 2005; Khazaei et al., 2014; Tan et al., 2015). Additionally, CRMP4L can interact with intersectin, an adaptor protein that regulates various cellular processes including endocytosis and exocytosis (Acheson et al., 1991; Yamabhai et al., 1998; Okamoto et al., 1999; Simpson et al., 1999; Hussain et al., 2001; Quinn et al., 2003). Thus, CRMP4L could play important roles in providing membrane and cell surface molecules important for axon regrowth. Consequently, CRMP4 could facilitate growth cone reformation in regenerating PNS axons, but also subsequent axon extension.

Conversely, loss of CRMP4 leads to a delay of Wallerian degeneration *in vitro.* The relative contribution of CRMP4 to growth of the proximal segment versus degeneration of the distal segment *in vivo* is an open question. In degenerating PNS axons, we observe the calpain-mediated cleavage of CRMP4 and concomitant down-regulation of CRMP4S. Intriguingly, the expression pattern of CRMP4S and tCRMP4 observed in the sciatic nerve located distal to the injury site is very reminiscent of the CRMP2 expression profile following injury (Touma et al., 2007; Lin et al., 2011; Wakatsuki et al., 2011; Zhang et al., 2016). In the case of CRMP2, its inactivation either by phosphorylation or calpain-mediated cleavage impairs its microtubule stabilizing effects. Thus, it is likely that CRMP4 cleavage is mediating both gain-of-function toxicity in response to the accumulation of NTF and CTF fragments as well as a loss of function phenotype (Touma et al., 2007; Lin et al., 2011; Wakatsuki et al., 2011; Zhang et al., 2016). Axon transport is disrupted in degenerating neurons, and overexpression of CRMP2 in axotomized cortical neurons rescues this defect and restores microtubule organization (Touma et al., 2007; Zhang et al., 2016). CRMP2 couples with tubulin heterodimers, proteins and organelles to kinesin, allowing their anterograde transport (Kawano et al., 2005; Kimura et al., 2005; Arimura et al., 2009). As CRMP4 is also downregulated in degenerating neurons, this protein could also be involved in the maintenance of neuronal integrity, via the regulation of either microtubule stabilization, axonal transport or other functions that remain to be further explored. Additionally, calpain-mediated cleavage of CRMP4 leads to the generation of tCRMP4 fragments that are sufficient to trigger axonal degeneration in wild-type DRG neurons, which express endogenous levels of full-length CRMP4. CRMP4 and other CRMP family members

assemble as hetero-tetramers to mediate their functions (Wang and Strittmatter, 1997). While it is likely that an excess of full-length CRMP4 expression would buffer against the deleterious effects of tCRMP4, it is also possible that tCRMP4 fragments could integrate in hetero-tetramers compromising their functionality. For example, CRMP2 and CRMP4 assemble as a complex, which coordinate actin and microtubule dynamics in the developing neurons (Tan et al., 2015). In addition to compromising cytoskeletal dynamics, cleavage fragments could affect CRMP-dependent roles in axon and mitochondrial transportconsequently promoting axonal fragmentation (Zhang et al., 2016).

The activity of cytoskeletal regulators is regulated by different kinases and upstream regulators in the regenerating and degenerating neurons (Girouard et al., 2018). Interestingly, these regulators also exhibit differential roles in the proximal and distal axon segments. MAP3K dual leucine zipper kinase 1 (DLK-1) functions through JNK and p38 MAP kinase to support transcriptional and translational events required for axon regeneration, while it regulates microtubules dynamics and energetics to favor degeneration of the distal axons (Miller et al., 2009; Watkins et al., 2013; Geden and Deshmukh, 2016). Additionally, nicotinamide mononucleotide acetyltransferase 1 (NMNAT1) is required for axonal integrity and as such, in regenerating neurons, NMNAT1 preserves mitochondria to promote neuroprotection and support regeneration whereas in degenerating neurons, it limits degeneration by blocking NAD^+ depletion (Chen et al., 2016; Sasaki et al., 2016). Thus, CRMP4, similarly to SCG10/STMN2 and CRMP2, could potentially act downstream of DLK-1 and NMNAT1, but this hypothesis will need to be further explored.

An interesting aspect of this study is the dichotomy between CRMP4 functions in the PNS compared to the CNS. CRMP4 plays an important role in the transduction of growth-inhibitory signals like MAIs and CSPGs (Alabed et al., 2007; Alabed et al., 2010; Nagai et al., 2012; Nagai et al., 2016). Following spinal cord injury, sensory neurons lacking CRMP4 exhibited enhanced growth in the dorsal horn consistent with desensitization to MAIs and CSPGs (Nagai et al., 2016). Thus, the presence of myelin-associated inhibitory proteins and inhibitory glial scar components in the CNS and their absence in the PNS likely explains the differential regulation of CRMP4 in the two systems. It is also apparent that, following spinal cord injury, CRMP4 is upregulated in the astrocytes surrounding the glial scar, whereas following peripheral nerve injury, CRMP4 is

predominantly localized to damaged axons (Jang et al., 2010; Nagai et al., 2015). This diverging expression pattern suggests that, in the CNS, CRMP4 might possess additional functions in non-neuronal cells that would contribute to the regeneration failure. While the restricted expression of CRMP4 in axons in the sciatic nerve suggests a neuron cell autonomous role for CRMP4 in PNS regeneration, a neuron-specific CRMP4 deletion would be required to fully rule out additional roles for CRMP4 in inflammation or Schwann cell biology.

In conclusion, we characterized a dual role for the cytoskeletal regulator CRMP4 in the neuronal response to PNS injury, as it favors neuronal regeneration by promoting axonal regrowth and by facilitating Wallerian degeneration. Interestingly, these functions are very reminiscent of the growth-promoting effects of CRMP4 characterized in developing neurons, but differ from its growth-inhibitory action in the adult CNS. Understanding these differing functions is critical to the development of novel strategies to promote functional recovery following neuronal injuries.

674 **References**

675

676 Acheson A, Barker PA, Alderson RF, Miller FD, Murphy RA (1991) Detection of brain-
677 derived neurotrophic factor-like activity in fibroblasts and Schwann cells: inhibition
678 by antibodies to NGF. Neuron 7:265-275.
679 Alabed YZ, Pool M, Ong Tone S, Fournier AE (2007) Identification of CRMP4 as a convergent
680 regulator of axon outgrowth inhibition. J Neurosci 27:1702-1711.
681 Alabed YZ, Pool M, Ong Tone S, Sutherland C, Fournier AE (2010) GSK3 beta regulates
682 myelin-dependent axon outgrowth inhibition through CRMP4. J Neurosci 30:5635-
683 5643.
684 Arimura N, Hattori A, Kimura T, Nakamuta S, Funahashi Y, Hirotsune S, Furuta K, Urano T,
685 Toyoshima YY, Kaibuchi K (2009) CRMP-2 directly binds to cytoplasmic dynein and
686 interferes with its activity. J Neurochem 111:380-390.
687 Bandtlow CE, Loschinger J (1997) Developmental changes in neuronal responsiveness to
688 the CNS myelin-associated neurite growth inhibitor NI-35/250. Eur J Neurosci
689 9:2743-2752.
690 Bisby MA, Chen S (1990) Delayed wallerian degeneration in sciatic nerves of C57BL/Ola
691 mice is associated with impaired regeneration of sensory axons. Brain Res 530:117-
692 120.
693 Bradke F, Fawcett JW, Spira ME (2012) Assembly of a new growth cone after axotomy: the
694 precursor to axon regeneration. Nat Rev Neurosci 13:183-193.
695 Brosius Lutz A, Chung WS, Sloan SA, Carson GA, Zhou L, Lovelett E, Posada S, Zuchero JB,
696 Barres BA (2017) Schwann cells use TAM receptor-mediated phagocytosis in
697 addition to autophagy to clear myelin in a mouse model of nerve injury. Proc Natl
698 Acad Sci U S A 114:E8072-E8080.
699 Brown MC, Lunn ER, Perry VH (1992) Consequences of slow Wallerian degeneration for
700 regenerating motor and sensory axons. J Neurobiol 23:521-536.
701 Brown MC, Perry VH, Hunt SP, Lapper SR (1994) Further studies on motor and sensory
702 nerve regeneration in mice with delayed Wallerian degeneration. Eur J Neurosci
703 6:420-428.
704 Bruck W (1997) The role of macrophages in Wallerian degeneration. Brain Pathol 7:741-
705 752.
706 Cha C, Zhang J, Ji Z, Tan M, Li S, Wu F, Chen K, Gong S, Guo G, Lin H (2016) CRMP4 regulates
707 dendritic growth and maturation via the interaction with actin cytoskeleton in
708 cultured hippocampal neurons. Brain Res Bull 124:286-294.
709 Chen L, Nye DM, Stone MC, Weiner AT, Gheres KW, Xiong X, Collins CA, Rolls MM (2016)
710 Mitochondria and Caspases Tune Nmnat-Mediated Stabilization to Promote Axon
711 Regeneration. PLoS Genet 12:e1006503.
712 Dubovy P, Klusakova I, Hradilova-Svizenska I, Joukal M (2018) Expression of Regeneration-
713 Associated Proteins in Primary Sensory Neurons and Regenerating Axons After
714 Nerve Injury-An Overview. Anat Rec (Hoboken) 301:1618-1627.
715 Erez H, Spira ME (2008) Local self-assembly mechanisms underlie the differential
716 transformation of the proximal and distal cut axonal ends into functional and
717 aberrant growth cones. J Comp Neurol 507:1019-1030.

718 Erturk A, Becker K, Jahrling N, Mauch CP, Hojer CD, Egen JG, Hellal F, Bradke F, Sheng M,
719 Dodt HU (2012) Three-dimensional imaging of solvent-cleared organs using 3DISCO.
720 Nat Protoc 7:1983-1995.
721 Frey E, Valakh V, Karney-Grobe S, Shi Y, Milbrandt J, DiAntonio A (2015) An in vitro assay to
722 study induction of the regenerative state in sensory neurons. Exp Neurol 263:350-
723 363.
724 Gamage KK, Cheng I, Park RE, Karim MS, Edamura K, Hughes C, Spano AJ, Erisir A,
725 Deppmann CD (2017) Death Receptor 6 Promotes Wallerian Degeneration in
726 Peripheral Axons. Curr Biol 27:890-896.
727 Geden MJ, Deshmukh M (2016) Axon degeneration: context defines distinct pathways. Curr
728 Opin Neurobiol 39:108-115.
729 Gerdts J, Summers DW, Sasaki Y, DiAntonio A, Milbrandt J (2013) Sarm1-mediated axon
730 degeneration requires both SAM and TIR interactions. J Neurosci 33:13569-13580.
731 Ghosh-Roy A, Wu Z, Goncharov A, Jin Y, Chisholm AD (2010) Calcium and cyclic AMP
732 promote axonal regeneration in Caenorhabditis elegans and require DLK-1 kinase. J
733 Neurosci 30:3175-3183.
734 Girouard MP, Bueno M, Julian V, Drake S, Byrne AB, Fournier AE (2018) The Molecular
735 Interplay between Axon Degeneration and Regeneration. Dev Neurobiol 78:978-990.
736 Huebner EA, Strittmatter SM (2009) Axon regeneration in the peripheral and central
737 nervous systems. Results Probl Cell Differ 48:339-351.
738 Huebner EA, Kim BG, Duffy PJ, Brown RH, Strittmatter SM (2011) A multi-domain fragment
739 of Nogo-A protein is a potent inhibitor of cortical axon regeneration via Nogo
740 receptor 1. J Biol Chem 286:18026-18036.
741 Hussain NK, Jenna S, Glogauer M, Quinn CC, Wasiak S, Guipponi M, Antonarakis SE, Kay BK,
742 Stossel TP, Lamarche-Vane N, McPherson PS (2001) Endocytic protein intersectin-l
743 regulates actin assembly via Cdc42 and N-WASP. Nat Cell Biol 3:927-932.
744 Jang SY, Shin YK, Jung J, Lee SH, Seo SY, Suh DJ, Park HT (2010) Injury-induced CRMP4
745 expression in adult sensory neurons; a possible target gene for ciliary neurotrophic
746 factor. Neurosci Lett 485:37-42.
747 Jiang SX, Kappler J, Zurakowski B, Desbois A, Aylsworth A, Hou ST (2007) Calpain cleavage
748 of collapsin response mediator proteins in ischemic mouse brain. Eur J Neurosci
749 26:801-809.
750 Johnstone AD, Hallett RM, de Leon A, Carturan B, Gibon J, Barker PA (2018) A novel method
751 for quantifying axon degeneration. PLoS One 13:e0199570.
752 Jones SL, Selzer ME, Gallo G (2006) Developmental regulation of sensory axon regeneration
753 in the absence of growth cones. J Neurobiol 66:1630-1645.
754 Kamber D, Erez H, Spira ME (2009) Local calcium-dependent mechanisms determine
755 whether a cut axonal end assembles a retarded endbulb or competent growth cone.
756 Exp Neurol 219:112-125.
757 Kawano Y, Yoshimura T, Tsuboi D, Kawabata S, Kaneko-Kawano T, Shirataki H, Takenawa T,
758 Kaibuchi K (2005) CRMP-2 is involved in kinesin-1-dependent transport of the Sra-
759 1/WAVE1 complex and axon formation. Mol Cell Biol 25:9920-9935.
760 Khazaei MR, Montcalm S, Di Polo A, Fournier AE, Durocher Y, Ong Tone S (2015)
761 Development of a cell permeable competitive antagonist of RhoA and CRMP4
762 binding, TAT-C4RIP, to promote neurite outgrowth. J Mol Neurosci 55:406-415.

763 Khazaei MR, Girouard MP, Alchini R, Ong Tone S, Shimada T, Bechstedt S, Cowan M, Guillet
764 D, Wiseman PW, Brouhard G, Cloutier JF, Fournier AE (2014) Collapsin response
765 mediator protein 4 regulates growth cone dynamics through the actin and
766 microtubule cytoskeleton. J Biol Chem 289:30133-30143.
767 Kilinc D, Peyrin JM, Soubeyre V, Magnifico S, Saias L, Viovy JL, Brugg B (2011) Wallerian-like
768 degeneration of central neurons after synchronized and geometrically registered
769 mass axotomy in a three-compartmental microfluidic chip. Neurotox Res 19:149-161.
770 Kimura T, Watanabe H, Iwamatsu A, Kaibuchi K (2005) Tubulin and CRMP-2 complex is
771 transported via Kinesin-1. J Neurochem 93:1371-1382.
772 Kowara R, Moraleja KL, Chakravarthy B (2006) Involvement of nitric oxide synthase and
773 ROS-mediated activation of L-type voltage-gated Ca2+ channels in NMDA-induced
774 DPYSL3 degradation. Brain Res 1119:40-49.
775 Kowara R, Chen Q, Milliken M, Chakravarthy B (2005) Calpain-mediated truncation of
776 dihydropyrimidinase-like 3 protein (DPYSL3) in response to NMDA and H2O2
777 toxicity. J Neurochem 95:466-474.
778 Leon S, Yin Y, Nguyen J, Irwin N, Benowitz LI (2000) Lens injury stimulates axon
779 regeneration in the mature rat optic nerve. J Neurosci 20:4615-4626.
780 Lewis GM, Kucenas S (2014) Perineurial glia are essential for motor axon regrowth
781 following nerve injury. J Neurosci 34:12762-12777.
782 Lin PC, Chan PM, Hall C, Manser E (2011) Collapsin response mediator proteins (CRMPs)
783 are a new class of microtubule-associated protein (MAP) that selectively interacts
784 with assembled microtubules via a taxol-sensitive binding interaction. J Biol Chem
785 286:41466-41478.
786 Liu W, Zhou XW, Liu S, Hu K, Wang C, He Q, Li M (2009) Calpain-truncated CRMP-3 and -4
787 contribute to potassium deprivation-induced apoptosis of cerebellar granule
788 neurons. Proteomics 9:3712-3728.
789 Mason MR, Lieberman AR, Grenningloh G, Anderson PN (2002) Transcriptional
790 upregulation of SCG10 and CAP-23 is correlated with regeneration of the axons of
791 peripheral and central neurons in vivo. Mol Cell Neurosci 20:595-615.
792 Meijering E, Jacob M, Sarria JC, Steiner P, Hirling H, Unser M (2004) Design and validation of
793 a tool for neurite tracing and analysis in fluorescence microscopy images. Cytometry
794 A 58:167-176.
795 Mietto BS, Mostacada K, Martinez AM (2015) Neurotrauma and inflammation: CNS and PNS
796 responses. Mediators Inflamm 2015:251204.
797 Miller BR, Press C, Daniels RW, Sasaki Y, Milbrandt J, DiAntonio A (2009) A dual leucine
798 kinase-dependent axon self-destruction program promotes Wallerian degeneration.
799 Nat Neurosci 12:387-389.
800 Mokarram N, Bellamkonda RV (2011) Overcoming endogenous constraints on neuronal
801 regeneration. IEEE Trans Biomed Eng 58:1900-1906.
802 Nagai J, Goshima Y, Ohshima T (2012) CRMP4 mediates MAG-induced inhibition of axonal
803 outgrowth and protection against Vincristine-induced axonal degeneration. Neurosci
804 Lett 519:56-61.
805 Nagai J, Takaya R, Piao W, Goshima Y, Ohshima T (2016) Deletion of Crmp4 attenuates
806 CSPG-induced inhibition of axonal growth and induces nociceptive recovery after
807 spinal cord injury. Mol Cell Neurosci 74:42-48.

808 Nagai J, Kitamura Y, Owada K, Yamashita N, Takei K, Goshima Y, Ohshima T (2015) Crmp4
809 deletion promotes recovery from spinal cord injury by neuroprotection and limited
810 scar formation. Sci Rep 5:8269.
811 Niisato E, Nagai J, Yamashita N, Abe T, Kiyonari H, Goshima Y, Ohshima T (2012) CRMP4
812 suppresses apical dendrite bifurcation of CA1 pyramidal neurons in the mouse
813 hippocampus. Dev Neurobiol 72:1447-1457.
814 Okamoto M, Schoch S, Sudhof TC (1999) EHSH1/intersectin, a protein that contains EH and
815 SH3 domains and binds to dynamin and SNAP-25. A protein connection between
816 exocytosis and endocytosis? J Biol Chem 274:18446-18454.
817 Quinn CC, Chen E, Kinjo TG, Kelly G, Bell AW, Elliott RC, McPherson PS, Hockfield S (2003)
818 TUC-4b, a novel TUC family variant, regulates neurite outgrowth and associates with
819 vesicles in the growth cone. J Neurosci 23:2815-2823.
820 Rosslenbroich V, Dai L, Baader SL, Noegel AA, Gieselmann V, Kappler J (2005) Collapsin
821 response mediator protein-4 regulates F-actin bundling. Exp Cell Res 310:434-444.
822 Sasaki Y, Nakagawa T, Mao X, DiAntonio A, Milbrandt J (2016) NMNAT1 inhibits axon
823 degeneration via blockade of SARM1-mediated NAD(+) depletion. Elife 5.
824 Shin JE, Geisler S, DiAntonio A (2014) Dynamic regulation of SCG10 in regenerating axons
825 after injury. Exp Neurol 252:1-11.
826 Shin JE, Miller BR, Babetto E, Cho Y, Sasaki Y, Qayum S, Russler EV, Cavalli V, Milbrandt J,
827 DiAntonio A (2012) SCG10 is a JNK target in the axonal degeneration pathway. Proc
828 Natl Acad Sci U S A 109:E3696-3705.
829 Simpson F, Hussain NK, Qualmann B, Kelly RB, Kay BK, McPherson PS, Schmid SL (1999)
830 SH3-domain-containing proteins function at distinct steps in clathrin-coated vesicle
831 formation. Nat Cell Biol 1:119-124.
832 Spira ME, Erez H (2013) From an Axon into a Growth Cone After Axotomy: A Model for
833 Cytoskeletal Dynamics. In: The Cytoskeleton: Imaging, Isolation, and Interaction
834 (Dermietzel R, ed), pp 237-263. Totowa, NJ: Humana Press.
835 Tan M, Cha C, Ye Y, Zhang J, Li S, Wu F, Gong S, Guo G (2015) CRMP4 and CRMP2 Interact to
836 Coordinate Cytoskeleton Dynamics, Regulating Growth Cone Development and Axon
837 Elongation. Neural Plast 2015:947423.
838 Torchilin VP (2008) Tat peptide-mediated intracellular delivery of pharmaceutical
839 nanocarriers. Adv Drug Deliv Rev 60:548-558.
840 Touma E, Kato S, Fukui K, Koike T (2007) Calpain-mediated cleavage of collapsin response
841 mediator protein(CRMP)-2 during neurite degeneration in mice. Eur J Neurosci
842 26:3368-3381.
843 Unsain N, Heard KN, Higgins JM, Barker PA (2014) Production and isolation of axons from
844 sensory neurons for biochemical analysis using porous filters. J Vis Exp.
845 Wakatsuki S, Saitoh F, Araki T (2011) ZNRF1 promotes Wallerian degeneration by
846 degrading AKT to induce GSK3B-dependent CRMP2 phosphorylation. Nat Cell Biol
847 13:1415-1423.
848 Waller A (1850) Experiments on the section of the glossopharyngeal and hypoglossal
849 nerves of the frog, and observations of the alterations produced thereby in the
850 structure of their primitive fibers. Philosophical transactions of the Royal Society of
851 London 140:423-429.
852 Wang KK (2000) Calpain and caspase: can you tell the difference? Trends Neurosci 23:20-
853 26.

Wang LH, Strittmatter SM (1997) Brain CRMP forms heterotetramers similar to liver dihydropyrimidinase. J Neurochem 69:2261-2269.

Watkins TA, Wang B, Huntwork-Rodriguez S, Yang J, Jiang Z, Eastham-Anderson J, Modrusan Z, Kaminker JS, Tessier-Lavigne M, Lewcock JW (2013) DLK initiates a transcriptional program that couples apoptotic and regenerative responses to axonal injury. Proc Natl Acad Sci U S A 110:4039-4044.

Yamabhai M, Hoffman NG, Hardison NL, McPherson PS, Castagnoli L, Cesareni G, Kay BK (1998) Intersectin, a novel adaptor protein with two Eps15 homology and five Src homology 3 domains. J Biol Chem 273:31401-31407.

Zhang JN, Michel U, Lenz C, Friedel CC, Koster S, d'Hedouville Z, Tonges L, Urlaub H, Bahr M, Lingor P, Koch JC (2016) Calpain-mediated cleavage of collapsin response mediator protein-2 drives acute axonal degeneration. Sci Rep 6:37050.

Zhang Z, Ottens AK, Sadasivan S, Kobeissy FH, Fang T, Hayes RL, Wang KK (2007) Calpain-mediated collapsin response mediator protein-1, -2, and -4 proteolysis after neurotoxic and traumatic brain injury. J Neurotrauma 24:460-472.

Figure legends

Figure 1. *Crmp4* deletion impairs the regeneration of sensory neurons following sciatic nerve injury. A) Maximal intensity projections of straightened *Crmp4*$^{+/+}$ *or Crmp4* $^{-/-}$ sciatic nerves at 3 DPI following crush injury stained with SCG10, a marker of the regenerating sensory neurons. The injury site is labelled by a dotted line and the extremity of the regenerating fibres is indicated by arrowheads. Scale bar, 500 µm. **B)** Quantification of the distance of regeneration of the SCG10+ sensory neurons at 3 DPI in *Crmp4*$^{+/+}$ and *Crmp4*$^{-/-}$ mice. Data is represented as the mean number of neurons per mm^2 +/- S.E.M. The difference between the genotypes is statistically significant (n=5-6; two-way ANOVA, p=0.0006).

Figure 2. The expression of CRMP4 is differentially regulated following CNS and PNS injury. A) Illustration of the sciatic nerve injury model utilized to examine the response to PNS injury. **B, C)** Immunoblot analysis of the CRMP4 expression pattern in DRG **(B)** and sciatic nerve **(C)** lysates from wild-type mice at 3 days following sciatic nerve transection. The nerve samples collected span either 0 to 3 mm distal, 0 to 3 mm proximal (proximal 1), or 3 to 6 mm proximal (proximal 2) to the injury site. The data is representative of results obtained from 7 mice. Open arrowhead: long CRMP4 isoform (CRMP4L; 75 kDa); arrow: short CRMP4 isoform (CRMP4S; 65 kDa); solid arrowhead: CRMP4 cleavage product (tCRMP4; 55 kDa). **D, E, F)** Representative images of longitudinal sections of intact and injured sciatic nerves to evaluate the co-localization of CRMP4 with Tuj1 **(D)**, S100 **(E)** and ED1 **(F)**, which are respectively markers of neurons, Schwann cells and macrophages. **G)** Diagram of the optic nerve injury model used to examine the response to CNS axotomy. **H, I)** Immunoblot analysis of CRMP4 expression in retina **(H)** and optic nerve **(I)** lysates at 3 days following optic nerve transection. The nerve portions analyzed span from either 0 to 2 mm distal or 0 to 2 mm proximal to the injury site in the optic nerves. The data is representative of 4 independent replicates. Open arrowhead: long CRMP4 isoform (CRMP4L; 75 kDa); arrow: short CRMP4 isoform (CRMP4S; 65 kDa); solid arrowhead: CRMP4 cleavage product (tCRMP4; 55 kDa). **J)** Representative images of longitudinal sections of intact and injured optic nerves to evaluate the co-localization of CRMP4 a/b with the neuronal marker Tuj1.

Figure 3. CRMP4 promotes growth of injured sensory neurons. A) Immunoblot analysis of CRMP4 expression in sciatic nerve lysates of wild-type mice at different times following sciatic nerve transection. Samples collected after sciatic nerve transection span either 0 to 3 mm distal, 0 to 3 mm proximal (proximal 1), or 3 to 6 mm proximal (proximal 2) to the injury site. Open arrowhead: long CRMP4 isoform (CRMP4L; 75 kDa); arrow: short CRMP4 isoform (CRMP4S; 65 kDa); solid arrowhead: CRMP4 cleavage product (tCRMP4; 55 kDa). The data is representative of results obtained from 7 mice. **B, C)** Representative pictures **(B)** and quantification **(C)** of the regrowth of dissociated E15-16 wild-type or *Crmp4*$^{-/-}$ DRG neurons plated in microfluidic devices at 24 h after axotomy indicated an impaired regrowth after axotomy in the *Crmp4*$^{-/-}$ DRG neurons. Data is represented as the mean neurite outgrowth per channel +/- S.E.M. (n=7-8, two-tailed Student t-test). Scale bar, 200 µm.

Figure 4. *Crmp4* deletion delays Wallerian degeneration *in vivo* and *in vitro*. A) Semi-thin cross-sections of the degenerating sciatic nerve at 36 HPI, 3 DPI or 7 DPI following sciatic nerve transection, or of the intact contralateral nerve, in *Crmp4*$^{+/+}$ or *Crmp4*$^{-/-}$ mice. Scale bar, 50 µm. **B)** Quantification of the mean number of intact myelin sheaths per µm^2 +/- S.E.M. in the *Crmp4*$^{-/-}$ sciatic nerves compared to the *Crmp4*$^{+/+}$ controls displayed in **(A)** (n=3-7; two-way ANOVA with Bonferroni's multiple comparison test). **C, D)** Representative pictures of the axons extending from DRG explants at a distance of 500 µm from the center of the explant stained with Tuj1 **(C)** and quantification **(D)** of the extent of degeneration in E12.5 *Crmp4*$^{+/+}$ or *Crmp4*$^{-/-}$ DRG explants at 5 h after axotomy. Data in the graph is represented as the mean index of degeneration +/- S.E.M. (n=9-10; two-tailed Student t-test). Scale bar, 100 µm. **E)** Representative images of intact E12.5 DRG explants or at 24 h following NGF withdrawal (anti-NGF). **F)** Curves of the area covered by axons of *Crmp4*$^{+/+}$ and *Crmp4*$^{-/-}$ DRG explants in the presence (NGF) or absence (anti-NGF) of NGF. The curves represent the mean +/- S.E.M. **C)** Mean +/- S.E.M. of the area covered by the axons at a distance of 700 µm from the center of the explants (as indicated by a dotted line in **(G)**) in the presence or absence of NGF. Data is normalized to *Crmp4*$^{+/+}$ grown in the presence of NGF (n=3; one-way ANOVA, Tukey's multiple comparison test).

Figure 5. Calpain-dependent cleavage of CRMP4 occurs in degenerating axons following injury. A, B) Immunoblot analysis of the calpain substrate fodrin in sciatic nerve **(A)** and optic

nerve **(B)** lysates collected at the indicated days post-injury (DPI). The arrowheads indicate the presence of fodrin breakdown products, which are present when calpain is active. **C)** Western immunoblot analysis of CRMP4 expression in lysates prepared from P4-7 rat DRG neurons and treated with calpain *in vitro*. **D, E)** Western immunoblot analysis of CRMP4 expression in axonal lysates prepared from wild-type **(D)** or *Caspase-3*$^{-/-}$ **(E)** E12.5 DRG explants grown on cell-filter inserts collected at 3 h after axotomy. DRG explants were treated with ALLN to inhibit calpain. **F)** Western immunoblot analysis of CRMP4 expression in lysates prepared from P4-7 rat DRG neurons that were treated for 5 h with either GST or GST-Nogo-22. Arrow: short CRMP4 isoform (CRMP4S; 65 kDa); solid arrowhead: CRMP4 cleavage product (tCRMP4; 55 kDa).

Figure 6. CRMP4 cleavage fragments promote axonal degeneration. A) Western immunoblot analysis of WT-CRMP4S or CRMP4S-T524A in the presence or absence of calpain. Arrow: short CRMP4 isoform (CRMP4S; 65 kDa); solid arrowhead: CRMP4 cleavage product (tCRMP4; 55 kDa). **B)** Coomassie staining of the TAT-CRMP4 peptides corresponding to the amino- (NTF) or carboxy- (CTF) terminal CRMP4 cleavage fragments. TAT-CRMP4-NTF and -CTF produce peptides of approximately 60 kDa and 10-12 kDa respectively. **C)** Representative confocal pictures and orthogonal projections illustrating the integration of the TAT peptides (red) in the axons stained with Tuj1 (green). Scale bar, 10 µM. **D, E)** Representative pictures **(D)** and quantification of the index of degeneration **(E)** following treatment of the axons for 8 h with 2.5 µM TAT-CRMP4 peptides or with TAT-RFP as a control. The data in the graph represents the average fold-change in the index of degeneration compared to TAT-RFP +/- S.E.M. (n=4; one-way ANOVA, Tukey's multiple comparison test). Scale bar, 50 µM. **F)** Quantification of the index of degeneration following treatment of the axons for 8 h with 2.5 µM TAT-or GST-CRMP4 NTF peptides, or with TAT-RFP and GST as controls. The data is shown as the average fold-change in the index of degeneration compared to TAT-RFP +/- S.E.M. (n=3; one-way ANOVA, Tukey's multiple comparison test).

Figure 7: Schematic model illustrating the expression profile of CRMP4 following PNS and CNS injury. A) In the intact sciatic and optic nerves, CRMP4S is strongly expressed, while levels of CRMP4L are very low. **B)** In the sciatic nerve fibres located proximal to the injury site, the expression of CRMP4S is maintained, while CRMP4L is modestly upregulated. This

964 expression pattern correlates with regeneration and contributes to axon extension. In the axons
965 segments located distal to the injury site, entry of calcium promotes the calpain-dependent
966 cleavage of CRMP4, leading to the formation of tCRMP4 and downregulation of full-length
967 CRMP4, which promotes Wallerian degeneration. **C)** In the optic nerve, CRMP4S is
968 downregulated, while tCRMP4 is upregulated in the axons proximal to the lesion site, correlating
969 with the formation of retraction bulbs and the inhibition of axon regeneration. In the axon
970 fragments located distal to the injury site, the presence of tCRMP4 is accompanied by a sustained
971 expression of CRMP4S.
972
973
974

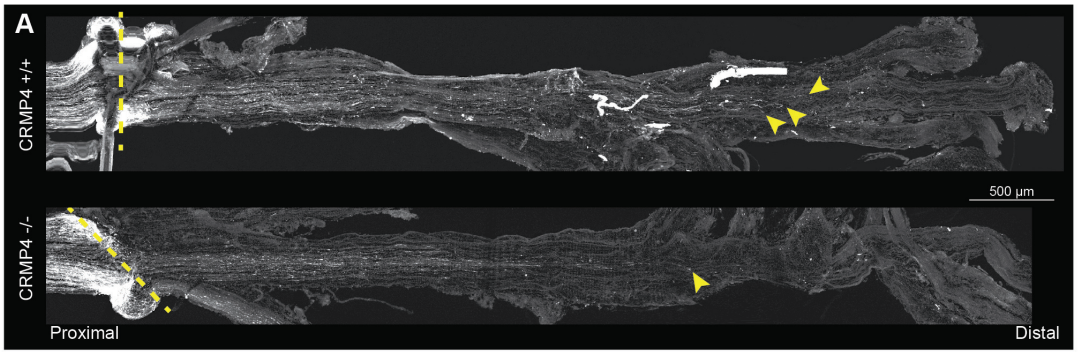

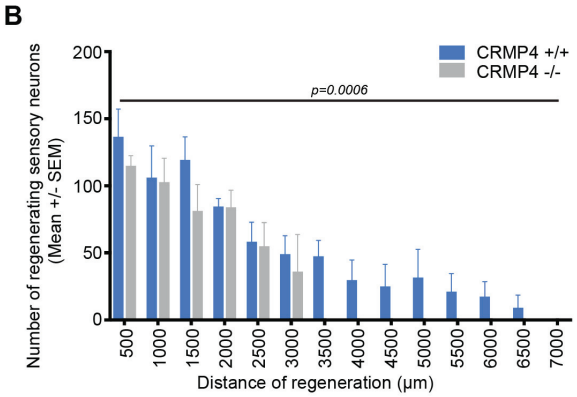

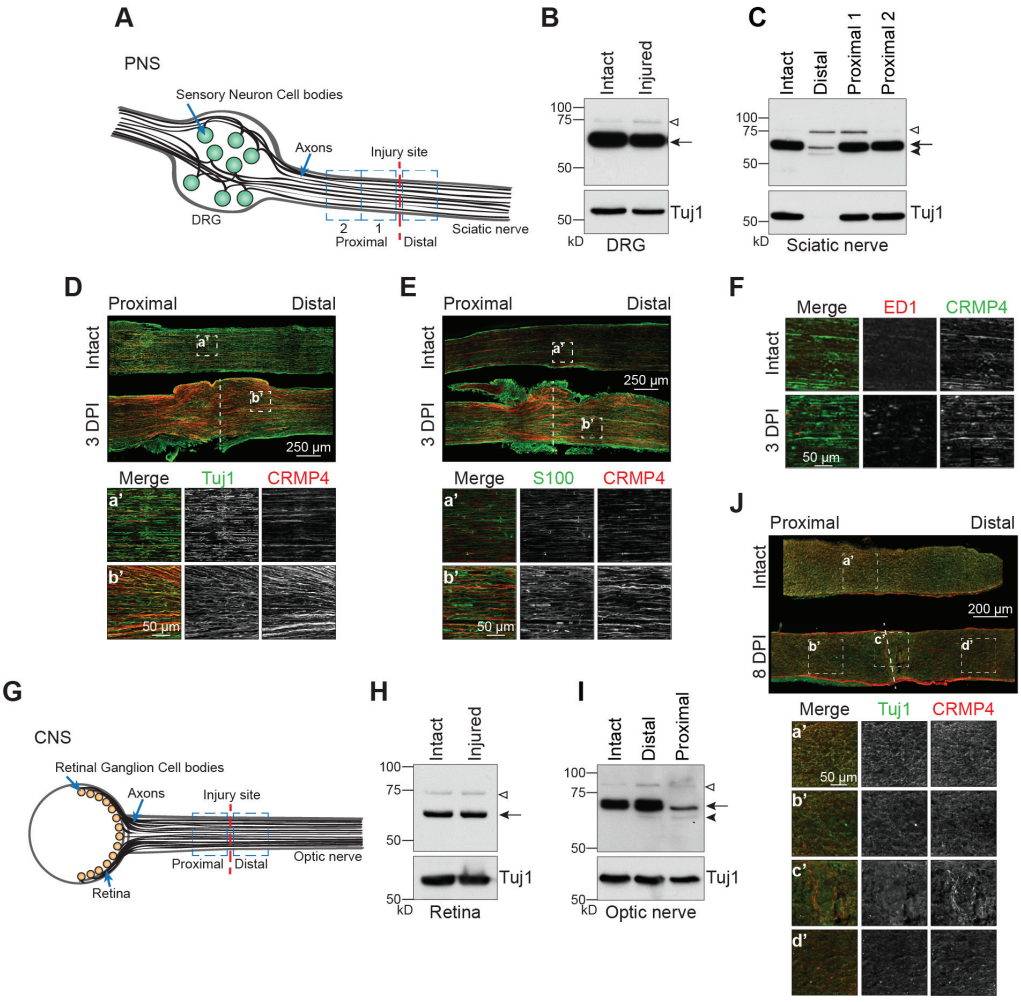

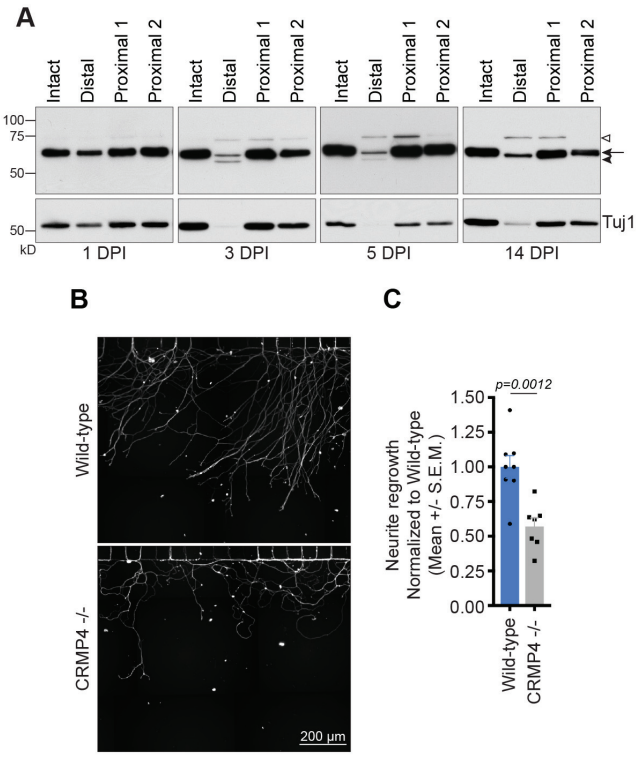

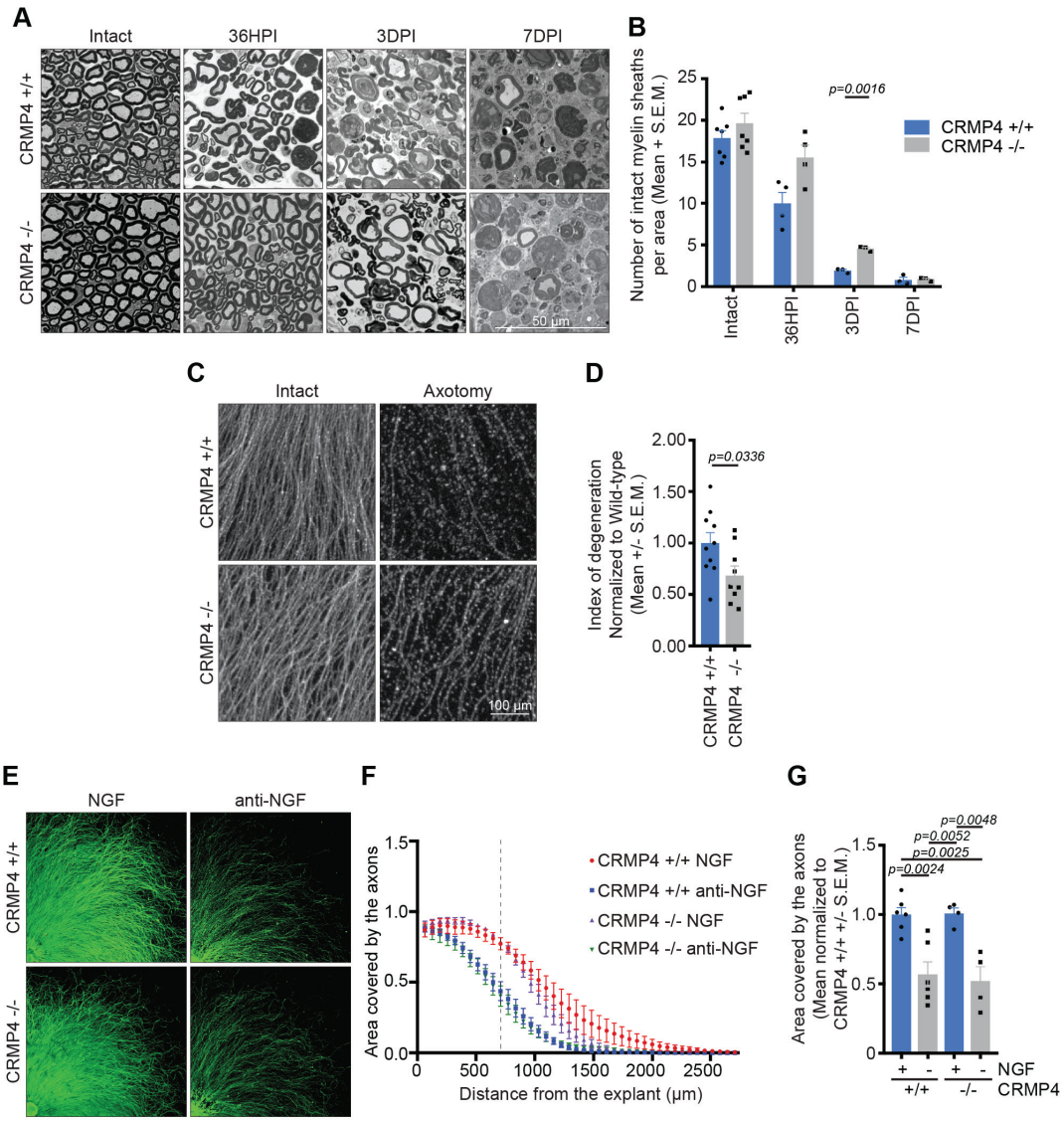

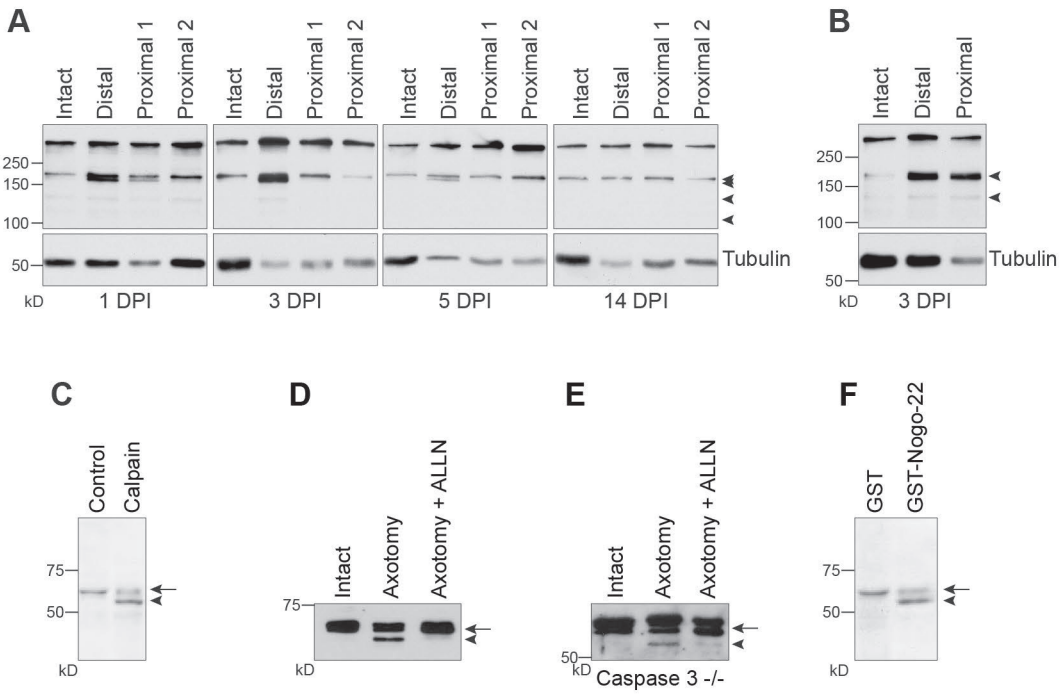

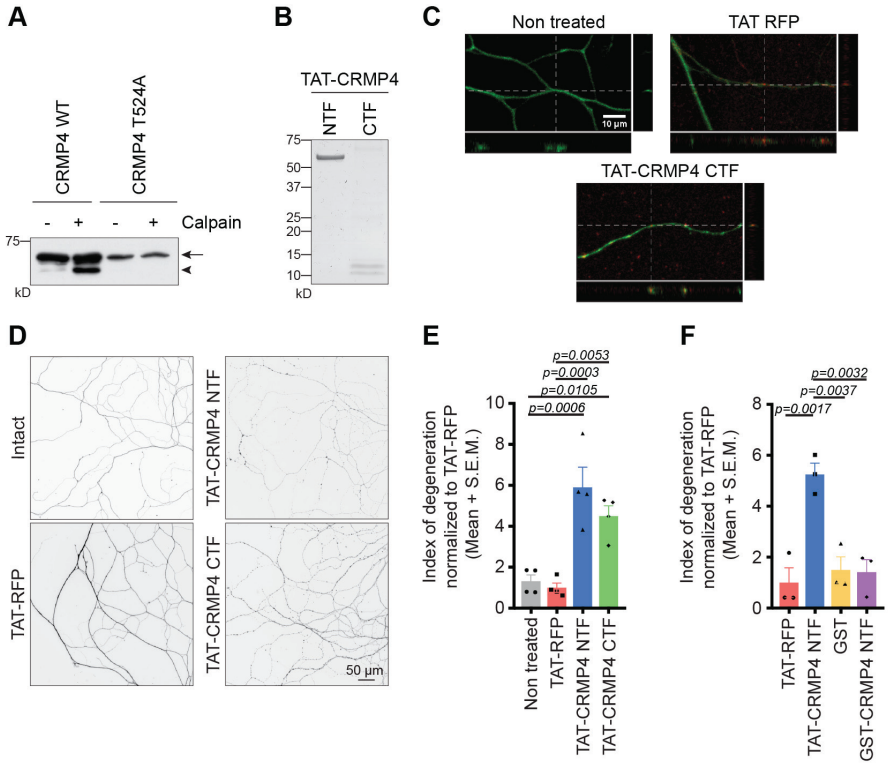

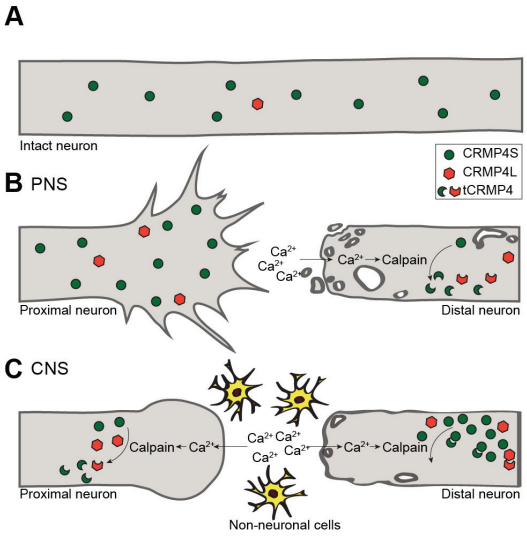

Table 1. Statistical tests

Figure	Data structure	Type of test	Sample size	Statistical data
Fig. 1B	Two factors (genotype and distance of regeneration)	Two-way ANOVA	$CRMP4^{+/+}$ mice: n=6; $CRMP4^{-/-}$ mice: n=5	Distance: $F_{(13,126)}=18.95$; $p<0.0001$; Genotype: $F_{(1,126)}=12.49$; p=0.0006; Interaction Genotype/Distance: $F_{(13,126)}=0.5537$; p=0.8860 Sidak's multiple comparison test: $CRMP4^{+/+}$ vs $CRMP4^{-/-}$ at all distances from the injury site: n.s.
Fig. 3C	Normal distribution	Unpaired Student t-test (two-tailed)	Wild-type DRG neurons: n=8; $CRMP4^{-/-}$ DRG neurons: n=7	t=;4.105; df=13; p=0.0012
Fig. 4B	Two factors (genotype and duration of degeneration)	Mixed effects analysis	For $CRMP4^{+/+}$ and $CRMP4^{-/-}$ mice: Intact sciatic nerves: n=7; Transected sciatic nerves at 36 HPI: n=4; Transected sciatic nerves at 3DPI and 7DPI: n=3	Time post-injury: $F_{(3,14)}=110.5$; Genotype: $F_{(1,12)}=8.569$; p=0.0127; Interaction Genotype/Time post-injury: $F_{(3,14)}=1.768$; p=0.1994 Sidak's multiple comparison test: Intact $CRMP4^{+/+}$ vs $CRMP4^{-/-}$ nerves: n.s.; Transected $CRMP4^{+/+}$ vs $CRMP4^{-/-}$ nerves at 36 HPI: n.s.; Transected $CRMP4^{+/+}$ vs $CRMP4^{-/-}$ nerves at 3 DPI: p=0.0016; Transected $CRMP4^{+/+}$ vs $CRMP4^{-/-}$ nerves at 7 DPI: n.s.
Fig. 4D	Normal distribution	Unpaired Student t-test (two-tailed)	$CRMP4^{+/+}$ explants: n=10; $CRMP4^{-/-}$ explants: n=9	t=2.311; df=17; p=0.0336
Fig. 6E	Normal distribution	One-way ANOVA	Wild-type DRG neurons: n=4	F=17.15; p=0.0001; $R^2=0.8109$ Tukey's multiple

Table 1. Statistical tests

				comparison test: Non-treated vs TAT-RFP: n.s.; Non-treated vs TAT-CRMP4 NTF: p=0.0006; Non-treated vs TAT-CRMP4 CTF: p=0.0105; TAT-RFP vs TAT-CRMP4 NTF: p=0.0003; TAT-RFP vs TAT-CRMP4 CTF: p=0.0053; TAT-CRMP4 NTF vs TAT-CRMP4 CTF: n.s.
Fig. 6F	Normal distribution	One-way ANOVA	Wild-type DRG neurons: n=3	F=15.06; p=0.0012; R^2=0.8496 Tukey's multiple comparison test: TAT-RFP vs TAT-CRMP4 NTF: p=0.0017; TAT-RFP vs GST: n.s.; TAT-RFP vs GST-CRMP4 NTF: n.s.; TAT-CRMP4 NTF vs GST: p=0.0037; TAT-CRMP4 NTF vs GST-CRMP4 NTF: p=0.0032; GST vs GST-CRMP4 NTF: n.s.
Fig. S1C	Normal distribution	One-way ANOVA	$CRMP4^{+/+}$ DRG explants: n=6; $CRMP4^{-/-}$ DRG explants: n=4	F=24.79; p<0.0001; R^2=0.8230 Tukey's multiple comparison test: $CRMP4^{+/+}$+NGF vs $CRMP4^{+/+}$-NGF: p=0.0024; $CRMP4^{+/+}$+NGF vs $CRMP4^{-/-}$+NGF: n.s.; $CRMP4^{+/+}$+NGF vs $CRMP4^{-/-}$-NGF: p=0.0025; $CRMP4^{+/+}$-NGF vs $CRMP4^{-/-}$+NGF: p=0.0052; $CRMP4^{+/+}$-NGF vs $CRMP4^{-/-}$-NGF: n.s.; $CRMP4^{-/-}$+NGF vs $CRMP4^{-/-}$-NGF:

Table 1. Statistical tests

				p=0.0048